Efficacious piezoelectric energy harvesting, including storage from low-frequency non-periodic bridge vibrations

Sumit Balguvhar[1], Suresh Bhalla[1,*] and Chee-Kiong Soh[2,3]

[1]Department of Civil Engineering, Indian Institute of Technology Delhi, Hauz Khas, New Delhi 110 016, India
[2]School of Civil and Environmental Engineering, Nanyang Technological University, Singapore
[3]School of Civil Engineering, Southeast University, Nanjing 211189, People's Republic of China

Although piezoelectric energy harvesting (PEH) from structural vibrations is well-recognized as a viable paradigm for renewable power generation in the micro- to milliwatt range, most real-life structures, such as bridges, are characterized by low-frequency erratic vibrations, which tend to diminish their practical utility for PEH. This is because the interface circuits involved in rectification and storage tend to lose their efficiency on account of low frequencies and the erratic nature of real-life structural vibrations. This study proposes a fine-tuned D1000 bridge rectifier circuit to circumvent the above problem, culminating in a successful proof-of-concept demonstration of PEH and subsequent storage in Ni–MH rechargeable batteries from real-life bridge vibrations. The unique feature of this experimental study entails successfully utilizing simple-type piezo elements directly bonded to the host structure and operating in the d_{31} mode. Additionally, piezo elements bonded to a secondary cantilever structure (acting as a parasite to the main structure) are studied for comparison. Here we present a laboratory-based experimental study of a bridge rectifier circuit for charging a battery from the energy harvested using piezoelectric elements. Results show that it is feasible to charge a battery under a low-frequency and low-voltage scenario ($V_{oc} = 1$ V at 5 Hz) employing the proposed D1000 rectifier circuit. We also present a field evaluation of the fine-tuned circuit on vibrations of a real-life flyover. Storage of energy in the capacitor as well as battery has been successfully realized in a realistic environment, achieving a power of 0.27 mW. This study represents successfully increasing the technology readiness level of PEH from 4 to 7 from structural vibrations.

Keywords: Battery storage, bridge, piezoelectric energy harvesting, rectifier circuit, structural vibrations.

WIRELESS sensor nodes (WSNs) deployed for the internet of things are powered by on-board batteries, which have a finite lifespan, thus limiting the functionalities of wireless sensing systems for applications in various sectors such as industry, military, civil infrastructure, etc.[1,2]. Replacement or recharging of batteries can be inconvenient and sometimes infeasible in remote hazardous locations. The power requirement of commercial ultra-low power WSNs employed for structural health monitoring (SHM) and data transmission range from 3–18 mW. Harvesting renewable energy is one of the essential technologies to realize true self-sustainable SHM by providing an alternate power source to WSNs. The theoretical concept of piezoelectricity is well known in the literature. In simplest terms, when a piezoelectric (PZT) patch is squeezed or elongated (i.e. mechanically strained), an electric charge accumulates at the electrodes. This is called the direct piezoelectric effect. The relationship between the voltage generated across the PZT patch and strain can be expressed as[3]

$$V = \left(\frac{d_{31}\overline{Y^{E_h}}}{\varepsilon_{33}^T} \right) S_1, \tag{1}$$

where d_{31} is the piezoelectric strain coefficient (Figure 1), S_1 the mechanical strain (along axis 1) and the electric field E_3 (along axis 3). Further, $\overline{\varepsilon_{33}^T} = \varepsilon_{33}^T(1-\delta j)$ is the complex electric permittivity (along axis 3) under constant stress, with $j = \sqrt{-1}$, and η and δ denote mechanical loss and dielectric loss factors of the piezoelectric material respectively. $\overline{Y^E} = Y^E(1+\eta j)$ is the complex Young's modulus of elasticity of the piezoelectric material.

Harvesters based on piezoelectric energy harvesting (PEH) are becoming popular because of the ease of scaling,
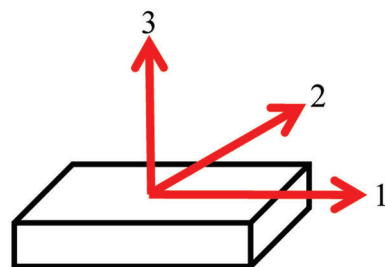
Figure 1. A typical piezoelectric plate patch with 1, 2 and 3 axes[27].

*For correspondence. (e-mail: sbhalla@civil.iitd.ac.in)

high power density and relatively high output voltage compared to the electro-magnetic and the electro-static systems[4]. In civil structures, such as city flyovers, vibration energy is abundantly available and can be utilized for energy harvesting using piezoelectric materials, which can directly convert mechanical strain to voltage signals without involving complex geometries or moving components. They are, however, characterized by non-periodic and low-frequency vibrations, often erratic, rendering the efficiency of the most diode and metal-oxide semiconductor field-effect transistor (MOSFET) circuits to as low as 12% (ref. 5).

Several studies have been made on energy harvesting from bridges – both steel and reinforced concrete (RC). Williams et al.[6] measured vibration data from bridges and applied them as an excitation source to a theoretical model based on an inductive generator to estimate the output power. Durou et al.[7] explored combined vibration and thermal energy harvesting, storing the generated electrical energy in a supercapacitor for powering SHM sensors on aircraft. It was concluded that vibration harvesting alone is not suitable to power SHM node. Still, it has the potential to supplement the solar harvesting system and make the system independent from daytime limitations. Zhou et al.[8] developed a wireless SHM system based on PEH. The sensor node used a cantilever-based piezoelectric device to harvest vibration energy and a microcontroller device to perform impedance-based SHM. However, when experimentally tested, the energy harvesting system could not generate enough power to run the SHM device. Kim et al.[9] conducted an experiment using an unimorph piezoelectric cantilever for energy harvesting. The piezoelectric module could generate about 13.8 V under cyclic loading of 10 kN. Ali et al.[10] theoretically estimated the possibility of power generation using a cantilever set-up for PEH. The results showed that the presence of mass decreased the output. However, real device development and experimentation were not performed. Peigney and Siegert[11] explored energy harvesting from traffic-induced bridge vibrations using a cantilever bimorph consisting of a tip mass and two Mide QP20W piezoelectric patches bonded to the clamped end of a steel plate. The cantilever was not directly bonded to the girder of the bridge but installed on a pipe fixed to the girder. The theoretical output power was predicted in terms of traffic intensity using a simple model, followed by experimental verification. Results showed that a power of 30 μW could be achieved at a frequency of 14.5 Hz. Kaur and Bhalla[3] demonstrated the feasibility of combined SHM and PEH from thin PZT patches in the form of a concrete vibration sensor (CVS) for RC structures. The power generated by the patch was 1.417 μW. Iqbal and Khan[12] developed a hybrid energy harvester by the combination of piezoelectric and electromagnetic systems. It comprises two cantilevers: the upper cantilever with a permanent magnet and the lower one holding a wound coil. Experimental results showed

the power achieved as 2.214 mW across 28 Ω at 0.6 g and 155.7 μW across 130 kΩ under 0.4 g. Wang et al.[13] proposed a generator for PEH from suspension structures. The energy was harvested through the bending patterns of the piezoelectric layers. The output peak power of 1.7 mW was achieved at a force loading of 120 g.

An important component of the PEH system is the interface circuit, which is usually deployed at the output of the piezo element in order to convert the voltage signal from alternating current (AC) to direct current (DC) and optimize the output power. Several types of electronic interface circuits have been proposed. Ottman et al.[14], used the concept of impedance matching and implemented an adaptive control technique to design an interfacing circuit. The circuit comprises an AC–DC rectifier and a DC–DC step-down converter operating in discontinuous conduction mode (DCM). The converter performed better at excitations producing voltages of 25 V or higher in the piezoelectric element compared to lower voltages. A variety of switch interface circuits have also been reported in the literature. Guyomar et al.[15,16] proposed a nonlinear technique known as synchronized switch harvesting on inductor (SSHI), which worked better for weakly coupled PEH systems[17,18]. The implementation of these elements involved complex circuitry and components for signal detection, switch operation, inductors and optimal load. A displacement sensor and a controller are necessary for synchronization and generation of the switching commands[19–21]. However, they consume higher power than the harvestable power, thus rendering them infeasible for practical applications. Lallart et al.[22] derived a rectifier using the series – SSHI and synchronized electric charge extraction (SECE) techniques, known as double synchronized switch harvesting (DSSH). The advantage of DSSH is that by tuning the ratio between the piezoelectric and the intermediate capacitor, the trade-off between the damping effects and the harvested energy can be controlled. Further improvement of the DSSH technique by Shen et al.[23] led to the concept of enhanced synchronized switch harvesting (ESSH).

The ESSH technique exhibited lower sensitivity to mismatch in the capacitance ratio and also provided finer control on the harvested energy. Kashiwao et al.[24] compared the bridge and double-voltage rectifier circuits for a vibration energy harvesting system using macro-fibre composite (MFC)-based piezo patches. The experimental results showed the power efficiency of the bridge circuit to be higher than that of the double-voltage rectifier circuit; however, the bridge circuit was found suitable at a low voltage only.

Past research on PEH considered secondary structures such as cantilever beams for harvesting energy. The main focus of previous studies was either on improving of the configurations of the secondary cantilever structure or the electronic interface circuits to scavenge maximum power from the generator[25]. Yet, a notable disconnect appears in

Table 1. Technology readiness level[26]

TRL	Definition
1	Physical principles are postulated with reasoning
2	Applications for physical principles identified, but no results
3	Initial laboratory tests on general hardware configurations to support physical principles
4	Integration level showing system functions in a laboratory test
5	System testing to evaluate functions in a realistic environment
6	Evaluation of the prototype system
7	Demonstration of the complete system in the operating environment
8	Certification testing on the final system in the laboratory and/or field
9	Final adjustment of the system through mission operations

Table 2. Efficiency comparison of various circuits

Circuit type	1 V, 5 Hz	1 V, 15 Hz	4 V, 5 Hz	4 V, 15 Hz
D1000	81.33%	72.55%	69.10%	62.55%
D5819	32%	39.09%	31.64%	44.04%
DMOS	9.3%	14.28%	9.37%	16.36%
GFCMOS	13.33%	25.18%	47.28%	52.24%
GCMOS	11.33%	20.30%	16.50%	23.22%

the knowledge of the effective electronic interface circuits and piezoelectric elements directly bonded to the host structure undergoing non-periodic (and often erratic) vibrations at very low frequencies (less than 5 Hz) for self-sustainable SHM applications. Roach and Neidigk[26] have classified the technology maturity level on a nine-point scale known as technology readiness level (TRL; Table 1). Currently, PEH for SHM is placed at level 4. According to the TRL scale, piezoelectric materials have been widely explored in laboratory-sized structures over the last few decades, but their potential in real-life civil structures has not been fully understood as well as demonstrated in real-life environment and is therefore not visible yet at the commercial level. In the present study, this aspect of PEH is addressed at the practical level in real-life structures.

This study presents laboratory and field experiments using a fine-tuned bridge rectifier circuit to demonstrate the feasibility of charging a rechargeable battery from the vibrations of a real-life city flyover using piezoelectric elements bonded directly on the girder. In such real-life structures, the signals are erratic and are characterized by low frequencies (<5 Hz) and low voltages (1–2 V). This proof-of-concept experimental study represents a rise in TRL from 4 to 7, which is the main contribution of this study.

Laboratory parametric studies

This section covers benchmark laboratory experiments for fine-tuning the storage of energy generated from the vibrations of piezoelectric elements (in a simple d_{31} configuration) in a rechargeable battery and the related parametric studies. A previous experimental study was conducted by us using capacitors[27]. A rechargeable battery is superior to

a capacitor since it ensures long-term power retention. Towards this end, experiments were conducted in the laboratory simulating real-life conditions of frequency and voltage. Recently, we have conducted an elaborate study involving a diode-based rectifier circuit (DBRC), MOSFET-based rectifier circuit (MBRC), gate cross-coupled rectifiers (GCMOS) and full gate cross-coupled MOSFET Rectifier circuit (FGMOS)[5]. The experiments were performed to harvest energy from an MFC piezo patch bonded to a cantilever beam which was subjected to various vibrational frequencies (5, 7, 9, 11, 13 and 15 Hz) and voltages (1, 2, 3 and 4 V) generally available in civil structures. Input signals were non-sinusoidal, resembling real-life scenarios.

The experimental results showed the best performance by D1000, a diode-based rectifier circuit, under all combinations of frequencies (5–15 Hz) and voltages (1–4 V) which are generally found in civil structures. Table 2 reproduces the efficiency demonstrated by various interface circuits. Charging efficiency of about 81.33% and harvestable power of 29.48 nW was achieved for 1 V open-circuit piezoelectric voltage at 5 Hz in case of D1000 circuit.

D1000 is a diode-based rectifier circuit comprising Schottky-type diodes, model BAT1000 (ref. 28). BAT1000 diodes are characterized by a lower-forward bias voltage of around 0.2 V. The forward bias voltage (V_f) can directly affect the output efficiency of the rectifier circuits. The topology consists of a bridge rectifier with an energy storage capacitor and the piezoelectric voltage source at the input (Figure 2). This is the simplest topology reported in the literature[29]. The four diodes labelled D_1 to D_4 are arranged in 'series pairs' with only two diodes conducting current during each half-cycle when the applied input voltage (V_{ac}) is greater than the diode threshold voltage (V_{th}). During the positive half-cycle of supply, D_1 and D_4 conduct in series, while D_2 and D_3 are reverse-biased and switched-off. On the other hand, during the negative half-cycle, D_3 and D_4 conduct in series, while D_1 and D_2 switch 'OFF' as they are now reversed biased. Utilizing a bridge rectifier is advantageous because it creates entirely passive circuit systems. The same has been employed in the present study by replacing the capacitor with a rechargeable battery.

Table 3. Properties of glass-fibre composite cantilever beam

Properties	Parameters	Glass-fibre composite cantilever beam
Geometrical properties	Length (mm)	220
	Cross section (mm^2)	35 × 1
	First natural frequency (Hz; theoretical)	4.39
Material properties	Young's modulus (Y^E; N/m^2)	12 × 10^9
	Density (kg/m^3)	5440

Table 4. Properties of aluminium cantilever beam

Properties	Parameters	Aluminium cantilever beam
Geometrical properties	Length (mm)	200
	Cross-section (mm × mm)	35 × 0.5
Material properties	Young's modulus (Y^E; N/m^2)	6.9 × 10^{10}
	Density (kg/m^3)	2715
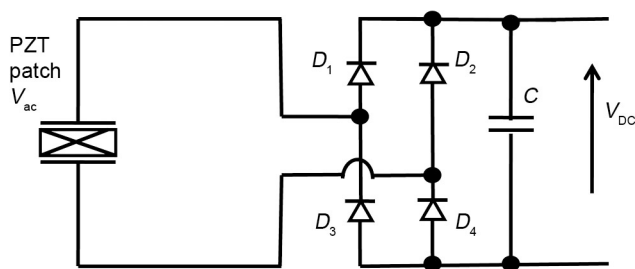
Figure 2. Bridge rectifier circuit.
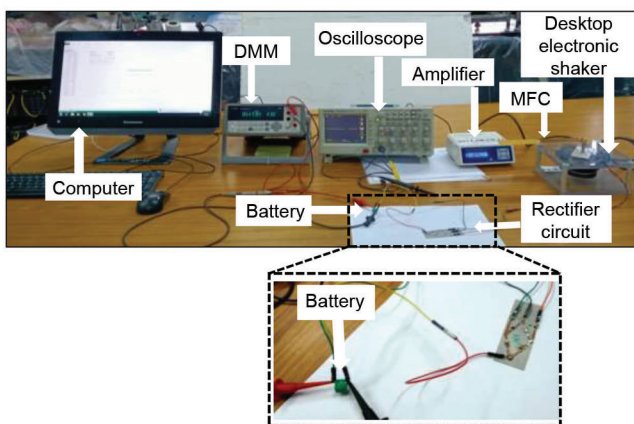
Figure 3. Experimental set-up for open circuit voltage from the macro-fibre composite (MFC) patch bonded to the cantilever beam.

Laboratory battery charging study

Figure 3 shows the experimental set-up to evaluate the performance of the D1000 rectifier circuit for charging a rechargeable battery. The set-up consists of an amplifier unit and a miniature shaker to excite the glass fibre composite cantilever beam (220 × 35 × 1 mm) provided by the manufacturer on the root of which the MFC patch of

size 85 × 28 × 0.3 mm is bonded to harvest the vibration energy[30] (Tables 3 and 4). To ensure charging and storing of energy in the battery and for better evaluation of the optimized circuit, low (1 V) as well as high (4 V) input voltage and frequency (5 and 10 Hz) scenarios were considered, and the same were generated using the desktop shaker and composite beam. The set-up was employed to generate voltages and frequencies closely matching the vibrations of the real-life flyover[27]. The D1000 rectifier circuit was connected to the output of the MFC patch, and a nickel–metal hydride (Ni–MH) rechargeable battery of 15 mAh was connected at the output of the rectifier circuit (see zoomed position, Figure 3) and allowed to charge to its full potential[31]. The Ni–MH battery was chosen because it has a high charge density compared to the lithium-ion battery and does not require any charge controller or voltage regulator. Key sight 34411A digital multimeter (DMM) was used to measure the voltage signals generated across the battery and charging time was recorded using the IntuiLink softwares which was operated in Excel format. Figure 4 shows the open-circuit voltage (V_{oc}) signal captured by the oscilloscope. It can be observed that the waveform has non-sinusoidal components resembling real-life bridge-type vibrations (Figure 5).

The experiment was conducted at a high open-circuit voltage, V_{oc} = 4 V and in low voltage scenarios, V_{oc} = 1 V at frequencies of 5 and 10 Hz to charge the battery. Figure 6 shows the charging curve of the battery at the two frequencies. It can be observed that when the cantilever is excited at 5 and 10 Hz at V_{oc} = 4 V, the battery is charged to a voltage of 2.52 V in 19,728 sec (5.48 h) and 3.10 V in 24,012 sec (6.67 h) respectively. It can also be seen from the figure that for V_{oc} = 1 V, at 5 and 10 Hz frequencies, the battery is charged to the final voltage of 0.88 V in 4320 sec (1.2 h) and 0.93 V in 5544 sec (1.54 h) respectively. In general, it can be concluded that as the excitation frequency and input voltage increase, the voltage across the battery also increases. However, it takes longer to charge as the frequency increases.

In order to determine the total energy stored in the battery by means of PEH, it was discharged by connecting a resistive load across the battery and monitoring the discharging process. Figure 7 shows the voltage discharging curve of the battery across a 4.7 kΩ resistor. It can be observed that when the battery is initially charged to 2.52 V (4 V, 5 Hz) and 3.10 V (4 V, 10 Hz) respectively, it can
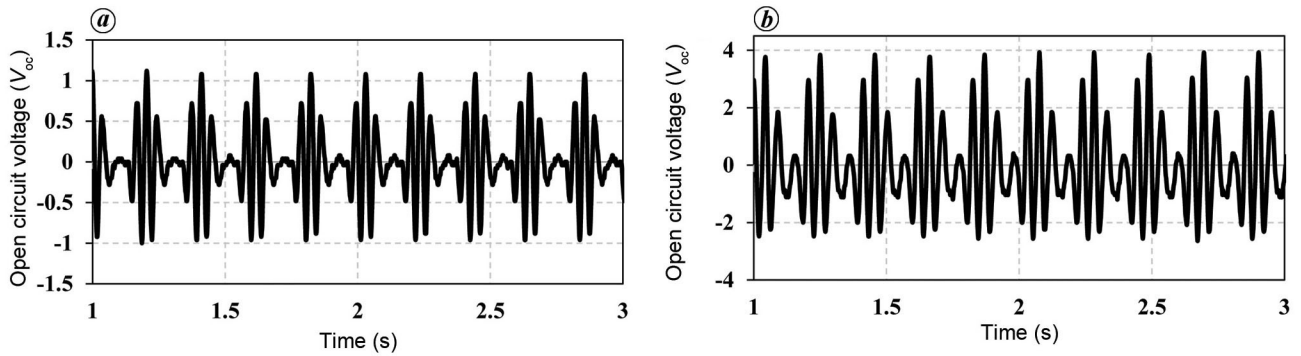
Figure 4. Typical open circuit voltage pattern (*a*) V_{oc} = 1 V and (*b*) V_{oc} = 4 V from the MFC patch bonded to the cantilever beam.
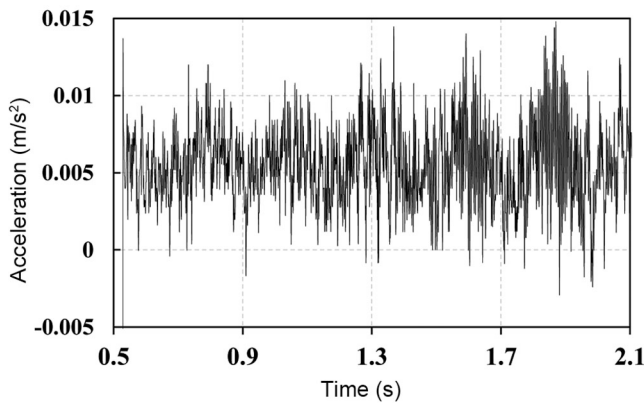
Figure 5. Time-domain plot of acceleration at midpoint of the side girder[27].

Figure 7. Discharging curve of the battery across a 4.7 kΩ load resistor for V_{oc} = 4 and 1 V at a frequency of 5 and 10 Hz.

Figure 6. Charging of battery from the MFC patch for V_{oc} = 4 V and 1 V at a frequency of 5 and 10 Hz.

power the load of a 4.7 kΩ resistor for 32,724 sec (9.09 h) and 40,464 sec (11.24 h) respectively. Similarly, if the battery is charged to 0.88 V (1 V and 10 Hz) and 0.93 V (1 V, 10 Hz) respectively, it can power the load of 4.7 kΩ resistor for 12,240 sec (3.40 h) and 15,120 sec (4.20 h) respectively. The total harvested energy (E_h) was determined as the area under the curve of power with respect to time, computed from Figure 7, by integration of the V_2/R function (Figure 8 *a*). It can be noted from

Figure 8 *a* that an energy of 19.77 J (10 Hz) and 29.65 J (5 Hz) is harvested for V_{oc} = 4 V and 0.65 J (10 Hz) and 0.72 J (5 Hz) for V_{oc} = 1 V. The average harvested power (P_{avg}; Figure 8 *b*), was determined by dividing the total harvested energy by the total charging time (T_c), as

$$P_{avg} = \frac{E_h}{T_c}. \tag{2}$$

It can be seen from Figure 8 *b* that 1 and 7 mW power is achieved for V_{oc} = 4 V at 5 and 10 Hz respectively. Similarly, 0.15 and 0.18 mW power is achieved for V_{oc} = 1 V at 5 and 10 Hz respectively. The experimental results show that it is feasible to charge the battery in the low-frequency and low-voltage scenario (V_{oc} = 1 V at 5 Hz) under non-periodic vibrations employing optimized D1000 rectifier circuit and harvesting power in the milliwatts range.

Next, we evaluated the D1000 rectifier circuit out using simple-type piezo patch from laboratory-based wind-induced vibrations, more or less representing the real-life pattern, to explore the possibility of storing energy in the rechargeable battery.
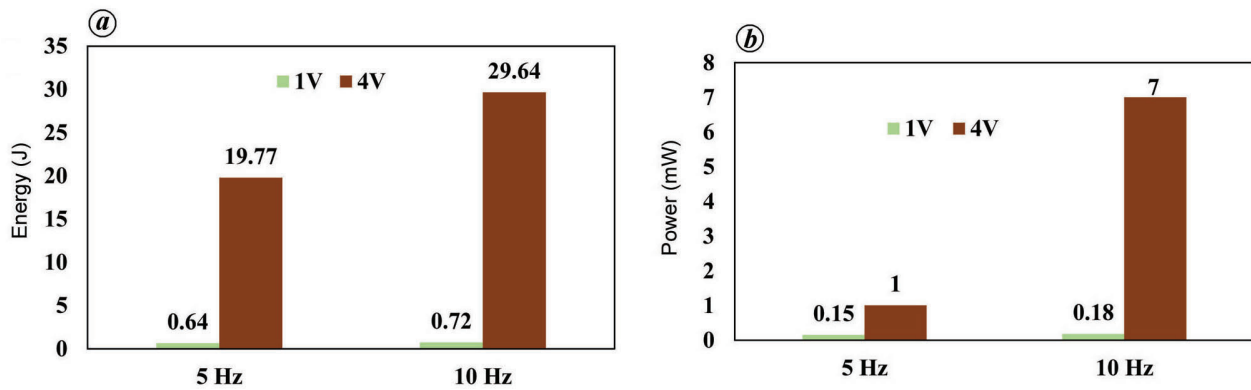
Figure 8. (*a*) Energy accumulated and (*b*) harvested power from the MFC patch at 5 and 10 Hz for V_{oc} = 1 and 4 V.
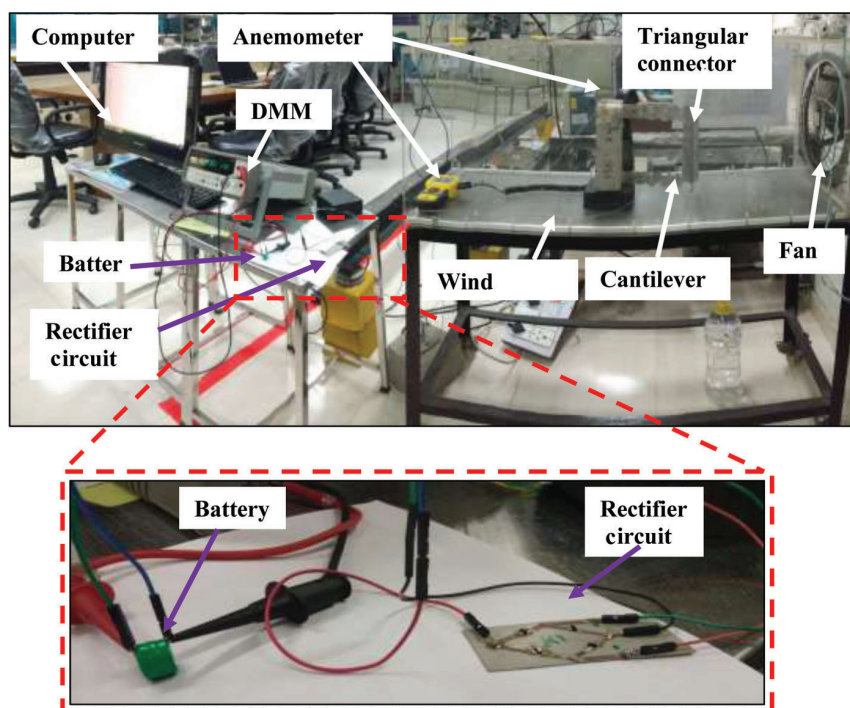
Figure 9. Experimental set-up for PEH from wind vibrations.

Experimental set-up for PEH from wind-induced vibrations

The experimental set-up consisted of a laboratory-sized (1 m long) wind tunnel and a chamber made of acrylic sheets (Figure 9). One end of the tunnel was open and the other end was fitted with an exhaust fan. The fan speed was controlled using a dimmer switch. A digital anemometer was used to measure wind velocity. The energy harvesting structure consisted of a pair of aluminium cantilever beams of size $200 \times 35 \times 0.5$ mm, joined together by a triangular connector, which enhanced the beam's fluttering (Figure 10). A PZT patch of size $10 \times 10 \times 0.3$ mm, grade PIC 151 (ref. 32), was bonded to the fixed side of an aluminium cantilever beam using standard Araldite

epoxy adhesive. Table 5 shows detailed material properties of the PZT patch, while Table 4 lists the properties of the aluminium cantilever beam. The D1000 rectifier circuit was connected to the output of the PZT patch. The Ni–MH rechargeable battery of 15 mAh was connected at the output of the rectifier circuit and allowed to charge to its full potential. The Keysight 34411A DMM was used to measure the voltage of the battery and charging time was recorded using the IntuiLink software.

Figure 11 *a* and *b* shows the typical open circuit voltage signals captured by the oscilloscope at the minimum speed of 1.6 m/s and a maximum speed of 3.2 m/s of the fan, corresponding to peak open voltage of 1 and 5 V respectively. The waveform has non-sinusoidal components. The fast Fourier transform (FFT) plots in Figure 12 *a* and
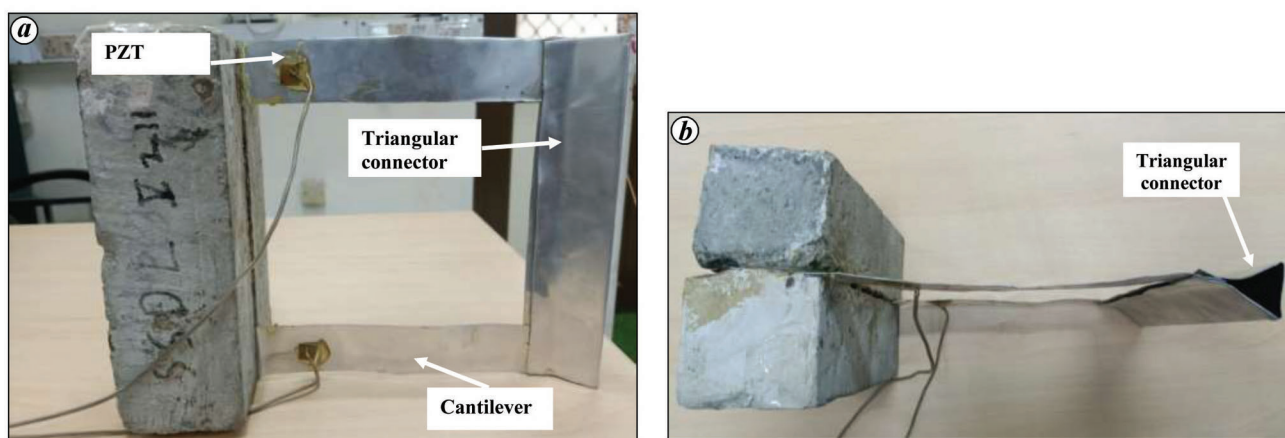
Figure 10. *a*, Structure of the harvester. *b*, Top view of the energy harvesting structure for wind induced vibrations.
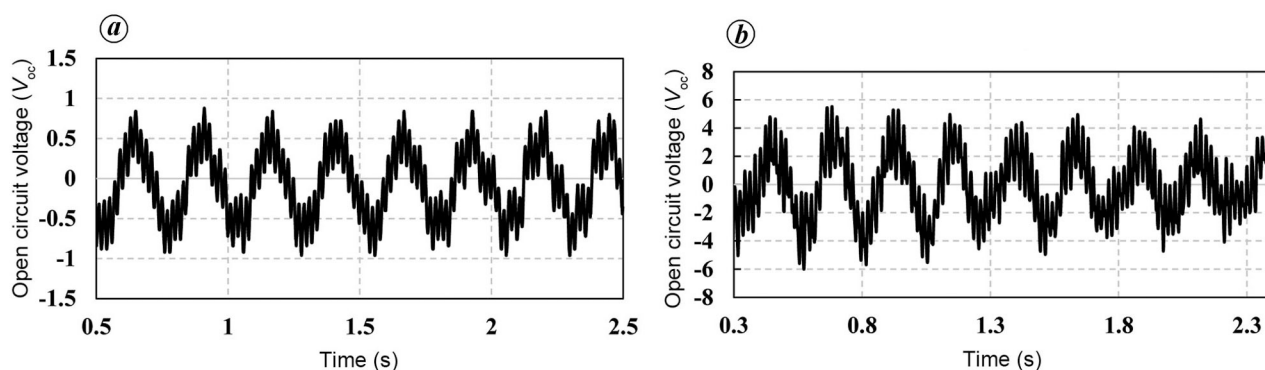
Figure 11. Typical open circuit voltage from the PZT patch bonded to the cantilever beam at (*a*) minimum wind speed of 1.6 m/s and (*b*) maximum wind speed of 3.2 m/s.

Table 5. Properties of the PZT patch and MFC patch[30,32]

Property	PZT	MFC
Plan size (mm²)	10×10	85×28
Thickness (h, mm)	0.3	0.3
Piezoelectric strain coefficient (d_{31}; m/V)	-2.10×10^{-10}	-1.71×10^{-10}
Young's modulus (Y^E; N/m²)	6.667×10^{10}	6.667×10^{10}
Electric permittivity (ε_{33}^T; F/m)	2.124×10^{-8}	8.85×10^{-12}

b at the minimum and maximum speed of the fan respectively, show that the induced frequency is 4 and 4.4 Hz respectively. Figure 13 *a* and *b* shows the charging curve of the battery from the PZT patch bonded to the cantilever corresponding to the minimum and maximum fan speed respectively. It can be observed that the battery is charged to the final voltage of 1.93 V in 26,532 sec (7.37 h) and 0.44 V in 15,840 sec (4.40 h) respectively, at the maximum and the minimum fan speed. Figure 14 *a* and *b* shows the voltage discharging curves of the battery across the 4.7 kΩ resistor. It can be observed that if the battery is charged to 1.93 and 0.44 V, it can power the load of the 4.7 kΩ resistor for 6.87 and 1.25 h respectively, when charged at the maximum and minimum fan speed. The total harvested energy and average harvested power were determined as 9.64 J and 0.36 μW for maximum fan speed respectively, and were 125 mJ and 7.9 μW for minimum fan speed respectively.

Thus, the charging of the battery has been successfully demonstrated from wind-induced vibrations using simple-type PZT patches. Power in microwatts range was achieved. This study shows the potential of wind-induced vibrations available in the exteriors as well as interiors (HVAC) for PEH. Next, we evaluated the optimized D1000 rectifier circuit in the field from traffic-induced vibrations of a real-life city flyover and explored the possibility of storing energy in the battery.

Field experiment: PEH from real-life traffic-induced vibrations

After successfully conducting laboratory experiments, the field experiment was carried out by considering the ambient vibrations of a real-life city flyover to evaluate the performance of an optimized rectifier circuit by charging a rechargeable battery in a realistic environment. The battery
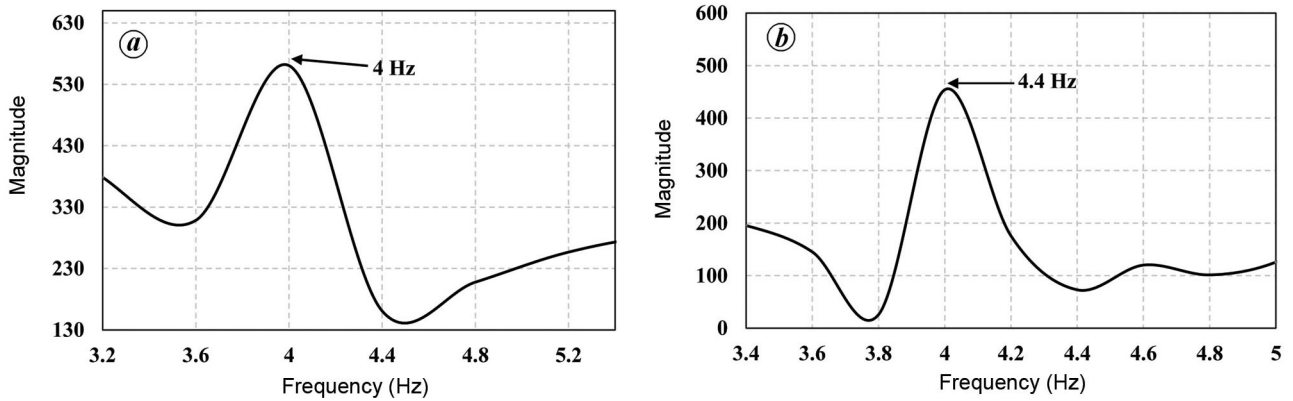
Figure 12. Frequency domain plot from the PZT patch bonded to the cantilever beam at minimum wind speed of 1.6 m/s and (***b***) maximum wind speed of 3.2 m/s.
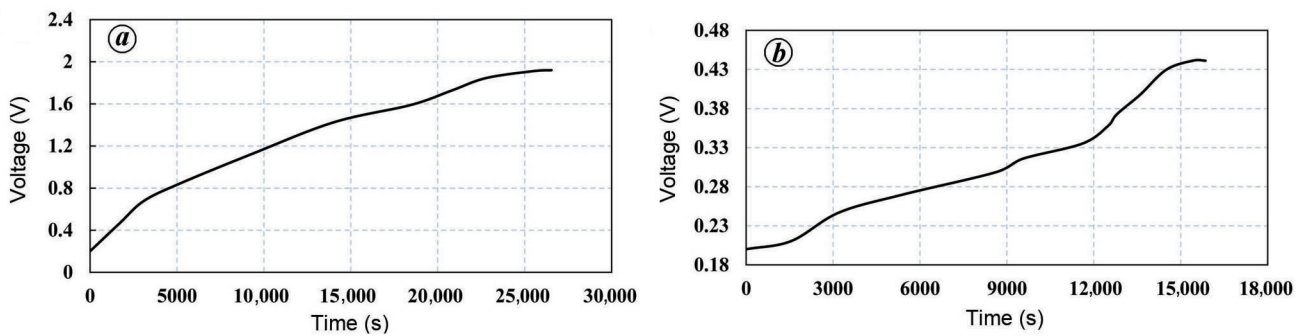
Figure 13. Charging curve of the battery at (***a***) maximum wind speed of 3.2 m/s and (***b***) minimum wind speed of 1.6 m/s.
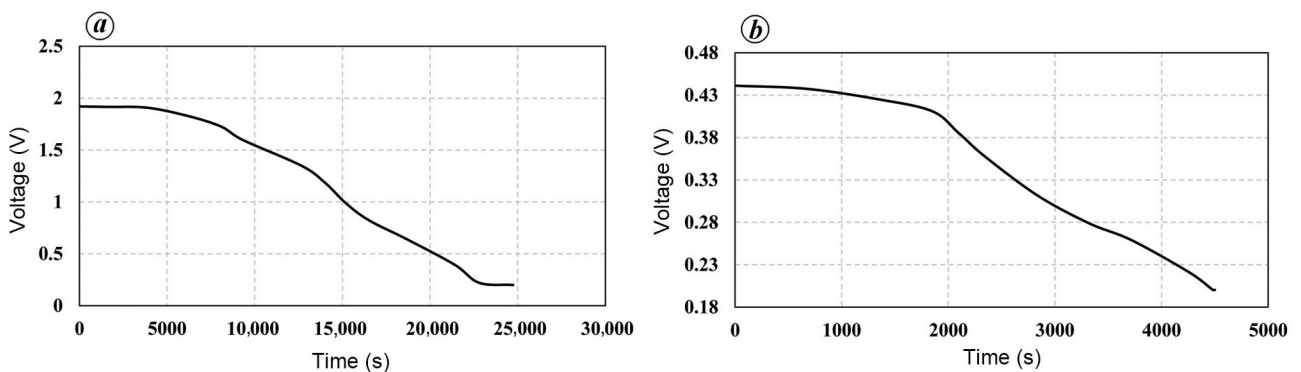
Figure 14. Discharging curve of the battery across the 4.7 kΩ load resistor for (***a***) maximum wind speed of 3.2 m/s and (***b***) minimum wind speed of 1.6 m/s.
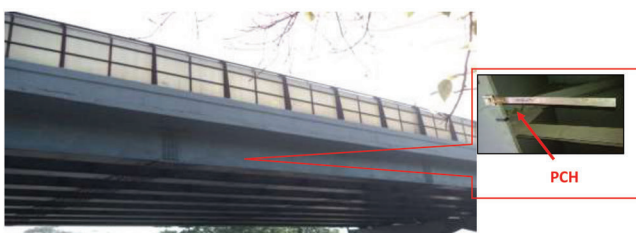
Figure 15. General view of the Jia Sarai flyover from the Indian Institute of Technology Delhi gate, India.

was charged in two ways: a piezoelectric cantilever harvester (PCH) attached to the bridge and piezoelectric patches bonded to the host structure. Both MFC-type and simple-type PZT patches were considered. The field experiment was conducted on the Jia Sarai flyover located in the vicinity of the Indian Institute of Technology Delhi (IIT-D), from which vibration measurements have been done previously by us[27]. It is a typical steel girder-type flyover with an RC deck (Figure 15). The portion selected
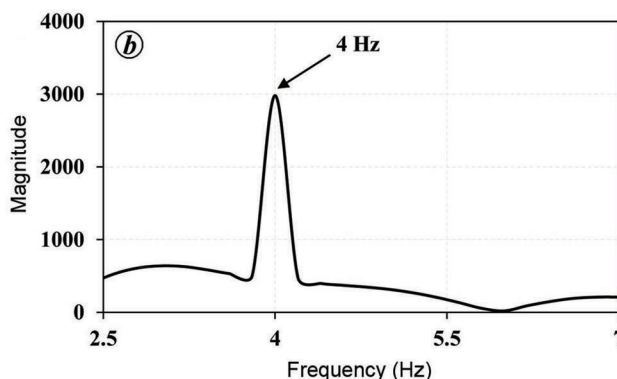
Figure 16. *a*, Piezoelectric cantilever harvester (PCH) with MFC. *b*, Frequency domain plot of PCH.

Figure 17. PCH with MFC piezo patch attached underneath the steel girder.
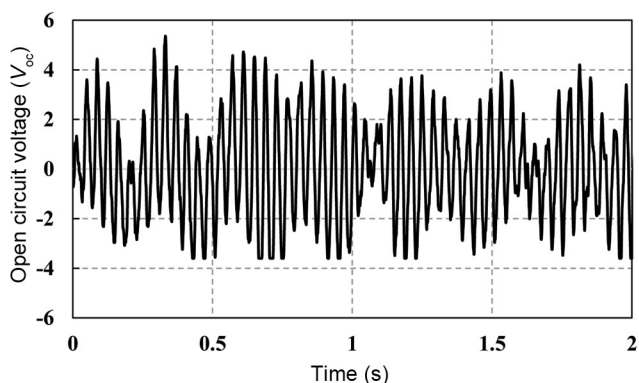
Figure 18. Plot of open circuit voltage from the MFC patch bounded to PCH as a function of time.

for the measurement has a girder depth of 2 m and a span of 28 m. In a previous study conducted on the same bridge, direct measurement of voltage and power was not made[27]. Acceleration was measured on the real bridge and the following equation was used to determine strain from acceleration[27]

$$S_{\mathrm{I}} = \frac{1.2 D_a}{\pi^2 L^2 f^2}, \tag{3}$$

where S_1 is the strain, D the girder depth, a the measured acceleration, L the bridge span and f is the frequency. Equation (1) was further used to determine peak voltage if a PZT patch was bonded. In the present study, however, direct measurement of voltage and power has been made from a PZT patch directly bonded to the bridge.

Installation of piezo patches

For the secondary structure mode, a stainless-steel PCH of size $450 \times 30 \times 1$ mm was chosen as the secondary structure. A commercially available MFC patch of size $85 \times 28 \times 0.3$ mm, Model M-8528-P2 (ref. 31), was bonded to the cantilever using standard Araldite epoxy adhesive (Figure 16 *a*). In order to achieve maximum efficiency, it was tuned to 4 Hz to match the fundamental frequency of the considered bridge. Figure 16 *b* shows the frequency domain response of PCH to an impact test measured using the MFC patch. From this, the natural frequency of PCH was found to be 4 Hz, which is the same as the dominant fundamental resonant frequency of the bridge. Figure 17 shows the installation of PCH underneath the girder with the help of a magnet. It was fixed to the midpoint of the exterior girder of the flyover facing the IIT-D side of the road. An open-circuit voltage of 4.5 V (average) was measured to be generated from the MFC patch bonded to the PCH when the bridge was under traffic (Figure 18), and continuous measurements were made for 2 h during the daytime.

In addition to PCH, a PZT patch of size $10 \times 10 \times 0.3$ mm, grade PIC 151 and an MFC patch of size $85 \times 28 \times 0.3$ mm, model M-8528-P2 were installed directly on the underside of the girder, adjacent to the PCH. Figure 19 shows the installation steps of the PZT patch on the girder. It was bonded to the underside of the girder using standard Araldite epoxy adhesive after cleaning the surface of the girder using sand-paper, covered with a plastic film and then pressed on the beam surface using a strong magnet for proper adherence (Figure 19 *a* and *b*). In this

way, 24 h of pressure curing was done. The patches were then soldered and covered with epoxy to protect the soldering (Figure 19 c and d). In the first attempt, the PZT patch had broken due to the high impact of the magnet over the patch (Figure 20). The installation of the piezoelectric element was successful after multiple attempts Figure 21 shows the steps involved in the instrumentation of the MFC patch directly onto the girder. The success rate is much higher for the MFC patch compared to the PZT patch.

Figure 22 a and b shows the typical time-domain plots of the open-circuit voltage generated from the PZT and MFC patches respectively. Peak voltages of 0.74 and 2.5 V were observed for the PZT patch and MFC patch respectively. The FFT of both signals revealed that the bridge's dominant fundamental resonant frequency was 4 Hz, matching the previously measured bridge frequency (Figure

23). It can be noted that the open-circuit voltage of 0.74 V generated from the PZT patch closely matches the estimated open circuit voltage of 0.78 V based on the measurement of acceleration in the previous study[27].

Field power measurements

Figure 24 shows the experimental set-up for charging a rechargeable battery using an optimized D1000 rectifier circuit from voltage signals generated from the sensors installed on the bridge. The oscilloscope was used to measure the output signals from the piezo elements. The Keysight 34411A DMM was used to measure the voltage across the battery, and charging time was recorded using the IntuiLink software. A portable generator was used for power supply to all the equipment used in the experiment. It was rested on the ground sufficiently far away from the bridge piers to ensure proper isolation of its vibration. In the field experiment, PCH was first used to measure the voltage signals from a real-life environment and evaluate the rectifier circuit by charging the battery. Thereafter, the PZT and the MFC patches directly bonded to the girder were evaluated. The D1000 rectifier circuit was used as the interface circuit for both patches. The Ni–MH rechargeable battery of 15 mAh capacity was then connected at the output of the rectifier circuit for charging to its full potential (Figure 24).

PEH from PCH: Figure 25 a and b shows the charging and discharging curves of the battery for the cantilever PCH. It can be observed from Figure 25 a that the battery is charged to the final voltage of 1.62 V in 26,856 sec (7.46 h). Figure 25 b shows that when charged to 1.62 V, it can power the load of the 4.7 kΩ resistor for 22,608 sec (28 h). From Figure 25 b, the total energy stored in the battery during charging was worked out by the integration
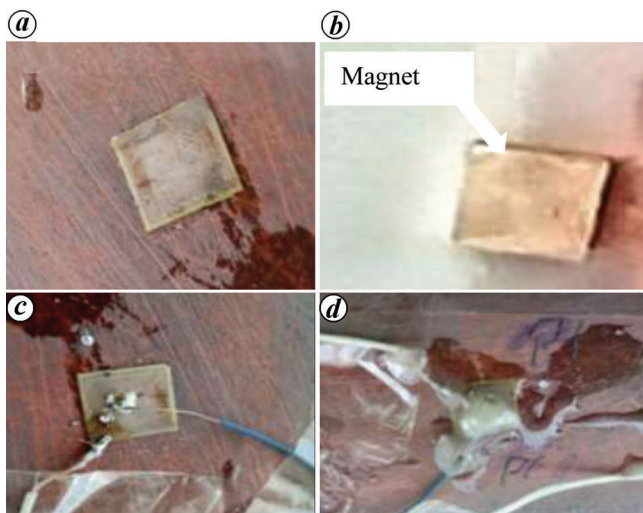
Figure 19. Installation steps for the PZT patch. *a*, PZT patch freshly pasted on epoxy layer. *b*, PZT patch covered with a magnet for curing. *c*, Connection wires soldered on the PZT patch after 24 h of curing. *d*, PZT patch covered with epoxy for protection.

Figure 20. Close up of broken PZT patch bonded to the girder.
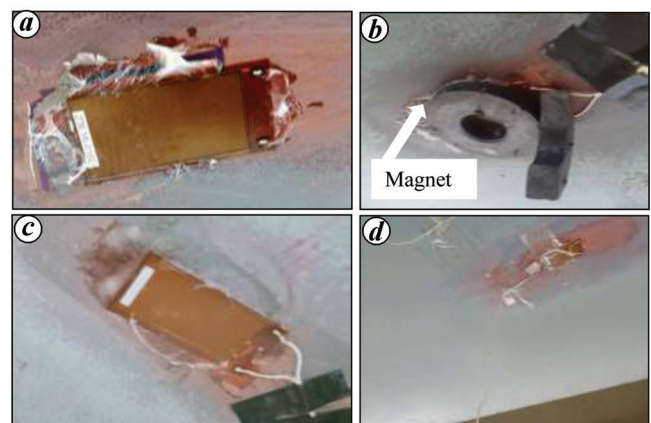
Figure 21. Installation steps for the MFC patch. *a*, MFC patch freshly pasted on the epoxy layer. *b*, MFC patch covered with a magnet for curing. *c*, Connection wires soldered on the MFC patch after 24 h of curing. *d*, MFC patch covered with epoxy for protection.
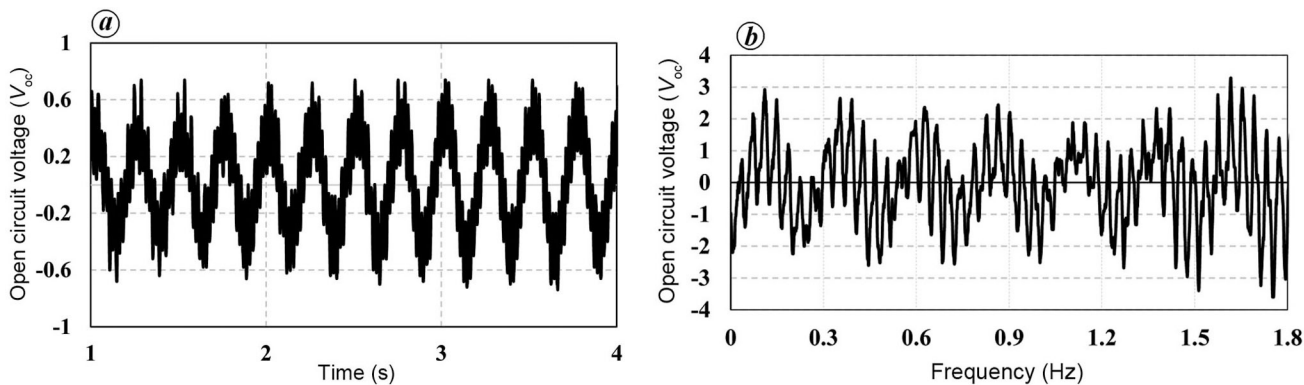
Figure 22. Typical open circuit voltage from (*a*) PZT patch and (*b*) MFC patch.
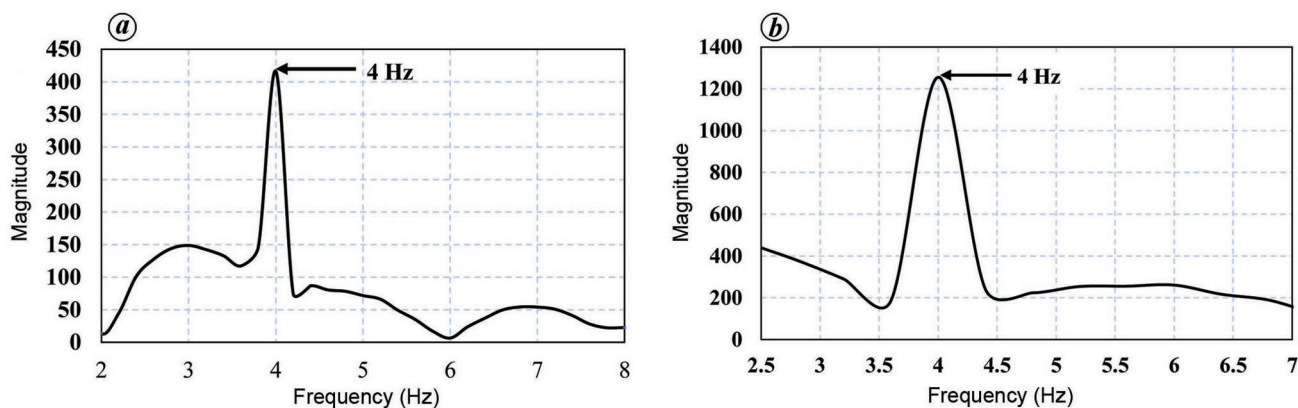
Figure 23. Frequency domain plot of voltage from (*a*) PZT patch and (*b*) MFC patch bonded to the girder.
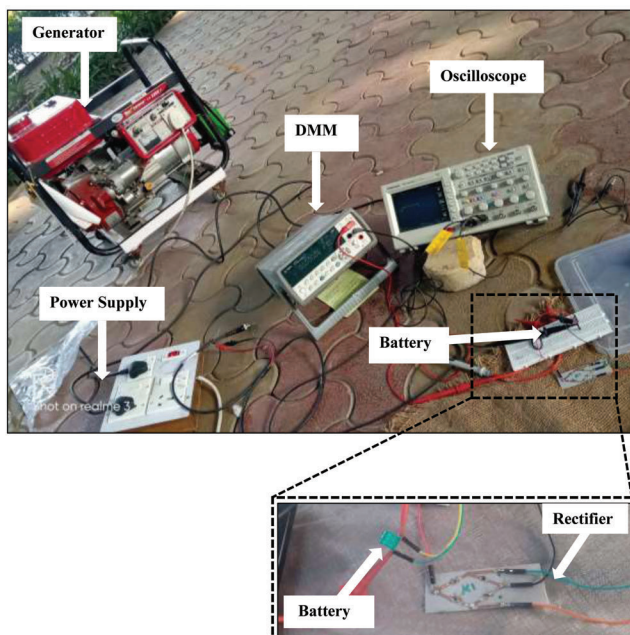
Figure 24. Experimental set-up for field power measurement.

of the V_2/R function with time. This was determined to be 7.46 J. The average harvested power from the PCH (P_{avg}) of 0.27 mW was determined using eq. (2). The experiment

establishes that the optimized D1000 rectifier circuit can be employed for PEH from real-life bridge vibrations. Next, measurements were carried out from the piezo patches (PZT and MFC) directly bonded to the girder.

PEH from directly bonded piezoelectric patches: Figure 26 *a* and *b* shows the charging curve of the battery from the MFC and PZT patches respectively, bonded directly to the girder. It can be observed that the battery is charged to the final voltage of 1.18 V in 29,088 sec (8.08 h) and 0.32 V in 17,496 sec (4.86 h) respectively, by the MFC and the PZT patches. Figure 27 *a* and *b* shows the discharging curves of the battery across the 4.7 kΩ resistor for the MFC and PZT patches. It can be observed that when the battery is charged to 1.18 and 0.32 V, it can power the load of the 4.7 kΩ resistor for 16,488 sec (4.58 h) and 1620 sec (0.45 h) respectively, for the MFC and PZT patches. The total harvested energy and average harvested power were determined as 5.13 J and 0.17 mW, 26 mJ and 1.56 µW, from the MFC and PZT patches respectively. Additionally, an electrolytic capacitor of 1 µF was charged to 0.6 V from the real-life bridge vibrations in 370 sec using the PZT patch (Figure 28). The energy per hour and average harvested power of 1.8 µJ and 0.5 nW respectively, were obtained.

In the field experiment an energy of 26 mJ had accumulated in the battery in case of the PZT patch at a minimum
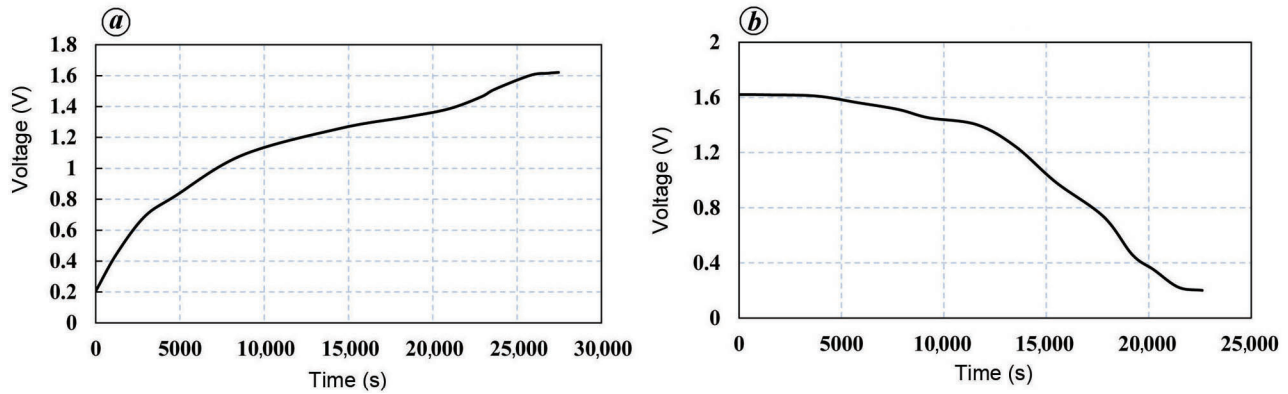
Figure 25. (*a*) Charging curve and (*b*) discharging curve of the battery across the 4.7 kΩ load resistor for PCH.
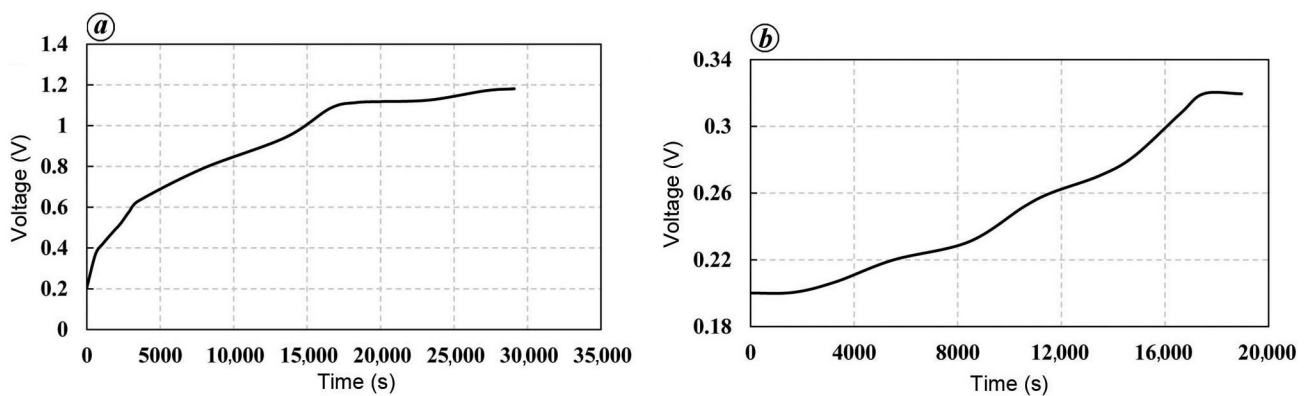
Figure 26. Charging of the battery from piezo patches bonded directly on the girder: (*a*) MFC patch and (*b*) PZT patch.
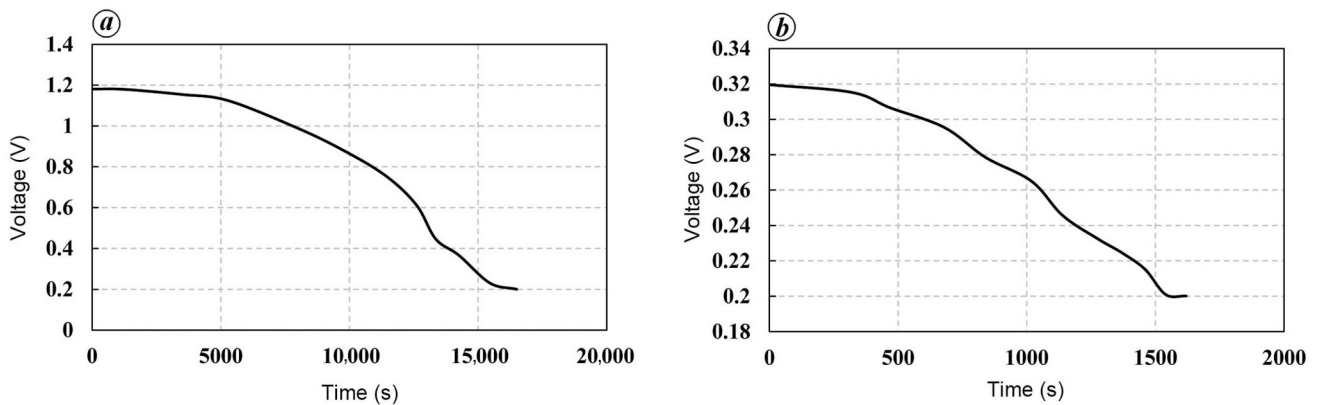
Figure 27. Discharging curve of the battery across the 4.7 kΩ load resistor for piezo patches bonded directly to the girder: (*a*) MFC patch and (*b*) PZT patch.

input voltage of 0.74 V and 4 Hz in 4.86 h (Figure 27 *b*). Based on this observation, the energy harvesting time required for the one-time operation of some typical ultra-low power-consuming electronic gadgets, such as digital temperature sensors, smoke detectors, impedance analysers (AD5933), etc. has been summarized (Table 6). It can be observed from Table 6 that continuous harvesting for 12 min from the real-life bridge vibrations using the PZT patch is sufficient for the one-time operation of a typical

A/D converter, such as TMP 112 (ref. 33), which requires energy of 25.2 µJ for a one-time operation. Similarly, for a typical CO/heat detector, such as E46C800 (ref. 34), 36 min is sufficient for a one-time operation. In addition, AD5933 (ref. 35) employed particularly for electro-mechanical impedance-based SHM, could be powered for one time with 6.16 h of harvested energy from the real-life bridge vibrations. Table 6 shows practical applications of PEH from a typical city flyover.

Table 6. Charging cycle of different circuits for various applications

| Circuit/IC | Energy required | 4 Hz at 0.78 V (26 mJ) | | Applications |
		Charging cycle	Charging time	
Typical A/D convertor, TMP 112 (ref. 34)	25.2 µJ	0	12 min (compared to Balguvhar and Bhalla[27])	Industrial applications
E46C800 (ref. 35)	3 mJ	0	36 min (compared to Balguvhar and Bhalla[27])	CO/heat detector
AD5933 (ref. 36)	33 mJ	1.26	6.168 h	Structural health monitoring

Table 7. Comparison of harvested power in the battery using MFC

Parameters	Laboratory experiment	Field experiment
Harvested power (mW)	0.15	0.17
Frequency (Hz)	5	4
Charging time (h)	1.20	8.08
Input voltage (V)	1	2.5
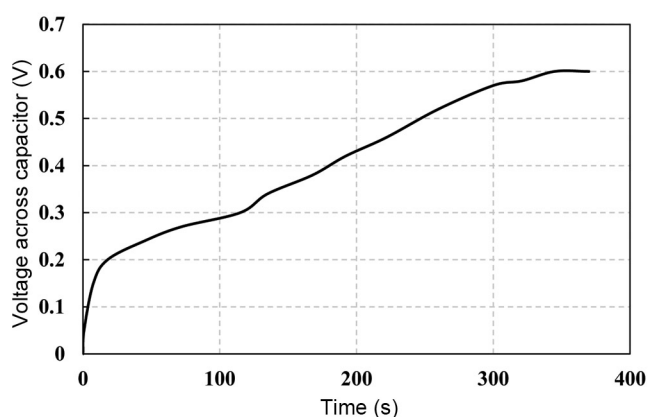
Figure 28. Charging of the capacitor from the PZT patch bonded directly to the girder.

Table 7 shows a comparison of laboratory and field experiments for harvested power accumulated in the battery using MFC under nearly the same condition of frequency (4 or 5 Hz). It can be seen from the table that harvested power achieved in the laboratory and field is 0.15 mW in 1.20 h and 0.17 mW in 8.08 h respectively. The reason for the long charging time in case of the field experiment despite higher voltage is due to the discontinuous and intermittent vibrations of the host structure. The power density (based on area) of the MFC patch (with an active area 23.8 cm^2) for laboratory and field experiments was 6.30 and 7.14 µW/cm^2 respectively. The power density was higher in the case of the field experiment compared to the laboratory experiment due to the higher impact factor of the moving load.

Conclusion

This study presents laboratory and field experiments of the D1000 rectifier circuit for charging a rechargeable battery with the energy harvested from a real-life bridge using the directly bonded piezoelectric elements. The output from the piezoelectric elements was fed directly to the D1000 rectifier circuit. A rechargeable battery of 15 mAh capacity was connected to the output of the circuit. The battery was allowed to charge to its full potential. Initial experiments were conducted in the laboratory simulating real-life conditions of low frequency and low voltage expected from civil structural vibrations. Harvested power of 1 and 7 mW for $V_{oc} = 4$ V, and 0.15 and 0.18 mW for $V_{oc} = 1$ V was achieved at 5 and 10 Hz respectively, from the MFC patch employing the optimized D1000 rectifier circuit. The next experiment was performed for charging the rechargeable battery with the energy harvested from wind induced vibrations using the piezoelectric elements. Harvested power of 0.36 and 7.9 µW was achieved for the maximum and minimum fan speed respectively. The field experiment for charging the rechargeable battery with the energy harvested from the real-life bridge vibration was carried out. A harvested power of 0.27 mW was achieved from PCH. The MFC and PZT patches bonded directly in the d_{31} configuration on the girder were evaluated for their energy harvesting potential. The harvested power was measured as 0.17 mW and 1.56 µW respectively, for the MFC and PZT patches. In addition to the battery, the capacitor could produce a power of 0.5 nW from the directly bonded PZT patch in the d_{31} configuration. The experimental results show that it is feasible to charge the battery under low-frequency (<5 Hz) and low-voltage scenarios ($V_{oc} = 1$ V), employing the optimized D1000 rectifier circuit. Thus, charging of the battery has been successfully demonstrated in a simple d_{31} configuration from a real-life structure. To the best of our knowledge, there have been no previous proof-of-concept real-life demonstrations of this kind.

In a nutshell, the feasibility of PEH and energy storage using piezoelectric elements bonded directly to the host structure operating in the d_{31} mode has been explored experimentally and successfully demonstrated in a realistic environment, i.e. a real-life bridge under operational conditions. This marks the establishment of a TRL of 7.0, which is the main contribution of this study.

1. Aabid, A. *et al.*, A systematic review of piezoelectric materials and energy harvesters for industrial applications. *Sensors*, 2021, **21**, 4145; https://doi.org/10.3390/s21124145.

2. Jiao, P., Egbe, K. J., Xie, Y., Nazar, A. M. and Alavi, A. H., Piezoelectric sensing techniques in structural health monitoring: a state-of-the-art review. *Sensors*, 2020, **20**, 3730; doi:10.3390/s20133730.

3. Kaur, N. and Bhalla, S., Combined energy harvesting and structural health monitoring potential of embedded piezo-concrete vibration sensors. *J. Energ. Eng.*, 2015, **141**(4), D4014001; 10.1061/(ASCE)EY.1943-7897.0000224.

4. Khaligh, A., Zeng, P. and Zheng, C., Kinetic energy harvesting using piezoelectric and electromagnetic technologies – state-of-the-art. *IEEE Trans. Ind. Electron.*, 2015, **57**(3), 850–860; 10.1109/TIE.2009.2024652.

5. Balguvhar, S., Piezoelectric energy harvesting through low frequency non sinusoidal vibrations of civil structures. Ph.D. thesis, Department of Civil Engineering, Indian Institute of Technology, Delhi, 2020.

6. Williams, C. B., Pavic, A., Crouch, R. S. and Woods, R. C., Feasibility study of vibration–electric generator for bridge vibration sensors. In Proceedings of 16th International Modal Analysis Conference, Santa Barbara CA, 2–5 February 1998, vol. 2, pp. 1111–1117.

7. Durou, H. *et al.*, Power harvesting and management from vibrations: a multi-source strategy simulation for aircraft structure health monitoring. In Proceedings of the SPIE Conference Smart Structures, Devices, and Systems IV, 2008, vol. 7268, pp. 1–10.

8. Zhou, D., Kong, N., Ha, D. S. and Inman, D. J., A self-powered wireless sensor node for structural health monitoring. In Proceedings of the 17th SPIE Annual International Symposium on Smart Structures and Materials and Non-destructive Evaluation and Health Monitoring, SPIE Smart Materials, Nano- and Micro-Smart Systems, Melbourne, Australia, 2008, vol. 7650, pp. 1–10.

9. Kim, S. H., Ahn, J. H., Chung, H. M. and Kang, H. W., Analysis of piezoelectric effects on various loading conditions for energy harvesting in a bridge system. *Sens. Actuator A*, 2011, **167**(2), 468–483; https://doi.org/10.1016/j.sna.2011.03.007.

10. Ali, S. F., Friswell, M. I. and Adhikari, S., Analysis of energy harvesters for highway bridges. *J. Intell. Mater. Syst. Struct.*, 2011, **22**(16), 1929–1938; doi:10.1177/1045389X11417650.

11. Peigney, M. and Siegert, D., Piezoelectric energy harvesting from traffic-induced bridge vibrations. *Smart Mater. Struct.*, 2013, **22**(9), 095019; doi:10.1088/09641726/22/9/095019.

12. Iqbal, M. and Khan, F. U., Hybrid vibration and wind energy harvesting using combined piezoelectric and electromagnetic conversion for bridge health monitoring applications. *Energ. Convers. Manage.*, 2018, **172**, 611–618; https://doi.org/10.1016/j.enconman.2018.07.044.

13. Wang, M. *et al.*, Piezoelectric energy harvesting from suspension structures with piezoelectric layers. *Sensors*, 2020, **20**, 3755; doi:10.3390/s20133755.

14. Ottman, G. K., Hofmann, H. F., Bhatt, A. C. and Lesieutre, G. A., Adaptive piezoelectric energy harvesting circuit for wireless remote power supply. *IEEE Trans. Power Electron.*, 2002, **17**(5), 669–176; doi:10.1109/TPEL.2002.802194.

15. Guyomar, D., Badel, A., Lefeuvre, E. and Richard, C., Toward energy harvesting using active materials and conversion improvement by nonlinear processing. *IEEE Trans. Ultrason., Ferroelectric. Freq. Control*, 2005, **52**(4), 584–595; doi:10.1109/TUFFC.2005.1428041.

16. Guyomar, D. and Lallart, M., Recent progress in piezoelectric conversion and energy harvesting using nonlinear electronic interfaces and issues in small scale implementation. *Micromachines*, 2011, **2**(2), doi:10.3390/mi2020274.

17. Shu, Y. C., Lien, I. C. and Wu, W. J., An improved analysis of the SSHI interface in piezoelectric energy harvesting. *Smart Mater. Struct.*, 2007, **16**(6), 2253–2264; doi:10.1088/0964-1726/16/6/028.

18. Lien, I. C., Shu, Y. C., Wu, W. J., Shiu, S. M. and Lin, H. C., Revisit of series-SSHI with comparisons to other interfacing circuits in piezoelectric energy harvesting. *Smart Mater. Struct.*, 2010, **19**(12), 125009; doi:10.1088/0964-1726/19/12/125009.

19. Liang, J. and Liao, W.-H., Energy flow in piezoelectric energy harvesting systems. *Smart Mater. Struct.*, 2010, **20**(1), 015005; doi:10.1088/0964-1726/20/1/015005.

20. Frey, A., Seidel, J., Schreiter, M. and Kuehne, I., Piezoelectric MEMS energy harvesting module based on non-resonant excitation. In 16th International Solid-State Sensors, Actuators and Microsystems Conference, 5–9 June 2011.

21. Lu, S. and Boussaid, F., A highly efficient P-SSHI rectifier for piezoelectric energy harvesting. *IEEE Trans. Power Electron.*, 2015, **30**(10), 5364–5369; doi:10.1109/TPEL.2015.2422717.

22. Lallart, M., Garbuio, L., Petit, L., Richard, C. and Guyomar, D., Double synchronized switch harvesting (DSSH): a new energy harvesting scheme for efficient energy extraction. *IEEE Trans. Ultrason., Ferroelectric. Freq. Control*, 2008, **55**(10), 2119–2130; doi:10.1109/tuffc.912.

23. Shen, H., Qiu, J., Ji, H., Zhu, K., Balsi, M. and Giorgio, I., A low-power circuit for piezoelectric vibration control by synchronized switching on voltage sources. *Sens. Actuator A*, 2010, **161**(1), 245–255; https://doi.org/10.1016/j.sna.2010.04.012.

24. Kashiwao, T., Izadgoshasb, I., Lim, Y. Y. and Deguchi, M., Optimization of rectifier circuits for a vibration energy harvesting system using a macro-fiber composite piezoelectric element. *Microelectronics J.*, 2016, **54**, 109–115; https://doi.org/10.1016/j.mejo.2016.05.013.

25. Priya, S. *et al.*, A review on piezoelectric energy harvesting: materials, methods and circuits. *Energy Harvest. Syst.*, 2017, **4**(1), 3–39.

26. Roach, D. and Neidigk, S., Does the maturity of structural health monitoring technology match user readiness? In Proceedings of the 8th International Workshop on Structural Health Monitoring, Stanford University, USA, 13–15 September 2011.

27. Balguvhar, S. and Bhalla, S., Evaluation of power extraction circuits on piezo-transducers operating under low-frequency vibration-induced strains in bridges. *Strain*, 2019, **55**(3), e12303; doi:10.1111/str.12303.

28. https://www.diodes.com/products/discrete/diodes-andrectifiers/diodes/schottky (accessed on 14 July 2021).

29. Anton, S. R. and Sodano, H. A., A review of power harvesting using piezoelectric materials (2003–2006). *Smart Mater. Struct.*, 2007, **16**(3), R1–R21.

30. https://www.smartmaterial.com/MFC-productmain.html (accessed on 11 July 2021).

31. https://www.varta-microbattery.com/en/products/nickel-metal-hydride (accessed on 14 July 2021).

32. PI Ceramic, Product Information Catalogue, Lindenstrabe, Germany; http://www.piceramic.de (accessed on 14 July 2021).

33. www.ti.com (accessed on 14 July 2021).

34. www.microchip.com (accessed on 14 July 2021).

35. Analog Devices, AD5933 Tech note, 2021; www.analog.com (accessed on 14 July 2021).